Deep convective cloud-top heights and their thermodynamic control during CRYSTAL-FACE

Steven C. Sherwood
Department of Geology and Geophysics, Yale University, New Haven, Connecticut, USA

Patrick Minnis
NASA/Langley Research Center, Hampton, Virginia, USA

Matthew McGill
NASA/Goddard Space Flight Center, Greenbelt, Maryland, USA

Received 24 March 2004; revised 21 July 2004; accepted 4 August 2004; published 30 October 2004.

[1] Infrared (11 μm) radiances from GOES-8 and local radiosonde profiles, collected during the Cirrus Regional Study of Tropical Anvils and Cirrus Layers-Florida Area Cirrus Experiment (CRYSTAL-FACE) in July 2002, are used to assess the vertical distribution of Florida-area deep convective cloud-top height and test predictions as to its variation based on parcel theory. The highest infrared tops (Z_{11}) reached approximately to the cold point at 15.4 km, though these are uncertain by about 1 km due to unknown cloud-environment temperature differences. Since lidar shows that visible "tops" are generally 1 km or more above Z_{11}, visible cloud tops frequently penetrated the lapse-rate tropopause (~15 km). Further, since tropospheric ice concentrations were typically present up to ~1 km above the visible tops, lofting of moisture through the mean cold point was probably common. Morning clouds, and those near Key West, rarely penetrated the tropopause. As in previous studies, nonentraining parcel theory fails to explain either of these results, though it does show promise in explaining day-to-day variations over the peninsula. Moisture variations above the boundary layer account for much of the day-to-day Z_{11} variability, especially over the oceans. In all locations a 20% increase in mean mixing ratio between 750 and 500 hPa was associated with about 1 km deeper maximum cloud penetration, other things being equal. This sensitivity is too large to explain by simple dilution of parcel buoyancy through mixing, implying microphysical or dynamical feedbacks on cloud development. The evident influence of midtropospheric humidity on the depth of the tropical troposphere suggests an interesting climate feedback possibility for stabilizing midtropospheric relative humidity. *INDEX TERMS:* 3314 Meteorology and Atmospheric Dynamics: Convective processes; 0368 Atmospheric Composition and Structure: Troposphere—constituent transport and chemistry; 1620 Global Change: Climate dynamics (3309); 3362 Meteorology and Atmospheric Dynamics: Stratosphere/troposphere interactions; 3374 Meteorology and Atmospheric Dynamics: Tropical meteorology; *KEYWORDS:* convection, tropical meteorology, tropopause

Citation: Sherwood, S. C., P. Minnis, and M. McGill (2004), Deep convective cloud-top heights and their thermodynamic control during CRYSTAL-FACE, *J. Geophys. Res.*, *109*, D20119, doi:10.1029/2004JD004811.

1. Introduction

[2] In the tropics, sufficient conditional instability is usually present for clouds to reach through most of the upper troposphere, at least according to nonentraining parcel theory. In fact, over the tropical western Pacific, it is true almost 90% of the time that CAPE (convective available potential energy) exceeds that of the "neutral" state toward which convection adjusts the column [*Sherwood*, 1999]. Tropical clouds are frequently observed to reach within a few kilometers of the tropopause, particularly in high-CAPE environments [e.g., *Jensen and Del Genio*, 2003]. It is generally assumed that greater quantities of CAPE (the potential energy available to a parcel of air through ascent through the unmodified environment, available for conversion to parcel kinetic energy) will lead to stronger convection. Measures of strength include greater updraft velocities and greater cloud-top heights. Estimated cloud heights serve as a proxy for convective strength and precipitation with reasonable success, as predicted by simple models [e.g., *Adler and Negri*, 1988].

[3] It is clear from previous measurements, however, that typical updraft velocities fall far short of the theoretical

0148-0227/04/2004JD004811$09.00

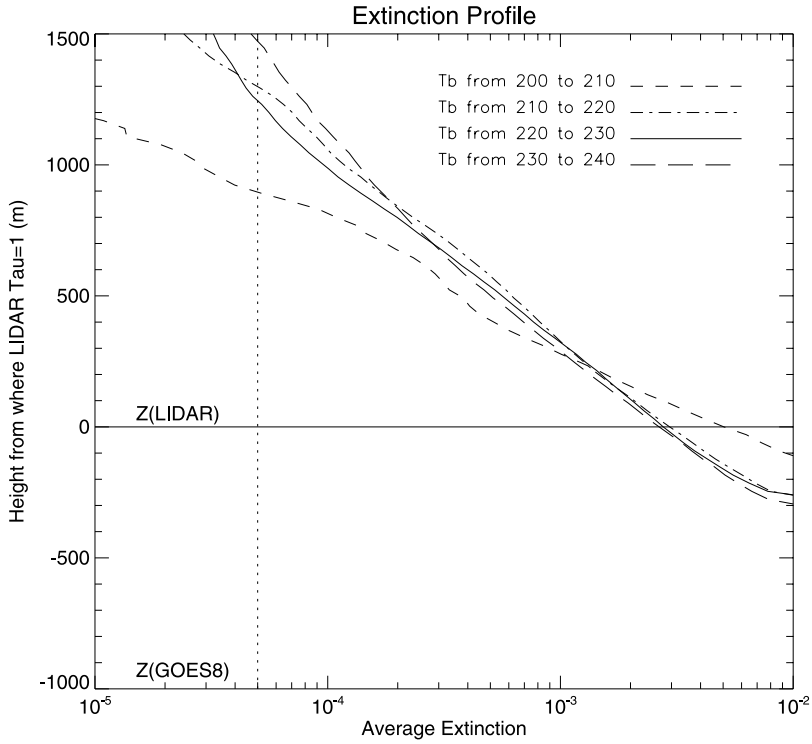

Figure 1. Mean extinction (in m^{-1}) calculated from the CPL for clouds in three T_{11} ranges indicated in the legend. Vertical coordinate is height above $Z_{lid}(1)$, the height at which lidar visible optical depth is unity, which is taken to be the visible cloud top. The average position of the GOES Z_{11} relative to this is also indicated, though this offset is approximate and appears to become greater than indicated as cloud tops approach the tropopause. The vertical dotted line indicates the extinction value corresponding to an ice water concentration equivalent to 5 ppmv, an approximate stratospheric value.

maxima, especially over oceans where the shortfall is typically more than an order of magnitude [*Jorgensen and Lemone*, 1989; *Lucas et al.*, 1994]. This indicates conversion of CAPE to parcel kinetic energy is often inefficient compared to an idealized, pseudoadiabatic process. The inefficiency is probably due to entrainment dilution and/or retention of condensed liquid in updrafts [e.g., *Jorgensen and Lemone*, 1989], although nonhydrostatic pressure effects could also play a role [*Chen and Sun*, 2002]. Simple cloud models that include these effects have been judged successful in predicting cloud-top heights and water content in case studies [*Ferrier and Houze*, 1989]. These issues are revisited in discussing our results (section 4.3).

[4] An understanding of what controls convective intensity is of interest for a number of reasons. For example, intense updrafts are responsible for the creation of hailstones and lighting. Lightning appears to require updraft strengths which, although well below those predicted for a pseudoadiabatic parcel, are greater than those actually achieved over oceans most of the time [*Zipser and Lutz*, 1994]. Thus the efficiency with which CAPE is converted to parcel kinetic energy is a key factor in regulating lightning and other severe storm characteristics. Further, considerable interest has developed in quantifying the extent of cloud penetration near the tropopause, to estimate in turn the degree of convective mixing or other effects at levels close to or within the lower stratosphere [e.g., *Gettelman et al.*, 2002; *Alcala and Dessler*, 2002]. Such mixing may cause transport of pollutants into the stratosphere [*Fromm and Servranckx*, 2003] and influence tropopause temperatures and moisture [*Johnson and Kriete*, 1982; *Sherwood et al.*, 2003; *Sherwood and Dessler*, 2001].

[5] Although typical updraft speeds are far below those predicted for an idealized parcel, the distribution of updraft speed is known to have a long tail, such that a few drafts are much stronger than average [*Yuter and Houze*, 1995b]. Since they are so rare, it is not clear from current data how well the behavior of the strongest updrafts may be controlled by parcel buoyancy in the prestorm environment. Though small in terms of storm area, the most intense drafts will likely dominate whatever role convection may play in mixing near the base of the stratosphere (a region that is otherwise very quiescent, with long dynamical and radiative timescales). Likewise, we may expect the tail of the cloud-height distribution to be more important than "average" heights. Study of this tail requires extensive sampling, for example by geostationary imagery.

[6] In July 2002, the CRYSTAL-FACE (Cirrus Regional Study of Tropical Anvils and Cirrus Layers-Florida Area Cirrus Experiment) employed numerous aircraft, surface, and space-based platforms to investigate the growth and decay of upper tropospheric cloud decks [*Jensen et al.*, 2004]. Here, we characterize the distribution of deep convective cloud-top heights that occurred during this experiment. We make no attempt to explain variations in the amount of convective activity, nor analyze individual cases

using radar vertical velocity data (whose availability is more limited than radiometric cloud-top data). Case studies of individual CRYSTAL convective events have been undertaken by *Li* [2003].

2. What is the "Cloud Top"?

[7] This question is not as simple as it seems. Our common experience is with clouds whose boundaries are either visibly sharp (liquid water cumulus clouds) or not easily visible at all (stratiform clouds). Though we might expect glaciated, deep convective clouds to have optically sharp tops too, this is not born out by lidar observations.

[8] Figure 1 shows data from the NASA Goddard Cloud Physics Lidar (CPL) on board the ER-2 high-altitude research aircraft. Each lidar dwell that encountered a deep convective cloud was composited relative to the level $Z_{\mathrm{lid}}(1)$ at which the optical depth (found by integrating the visible extinction) was equal to unity; such composites were developed for several brightness temperature ranges corresponding to different cloud heights in the upper troposphere. The $Z_{\mathrm{lid}}(1)$ level is the most sensible definition of a radiometric "cloud top," since it lies at the mean penetration depth of a (visible) photon.

[9] The figure shows two interesting things. First, cloud water content decays exponentially above $Z_{\mathrm{lid}}(1)$ with an *e*-folding distance of about 200 m. This decay continues for quite a few cloud "scale heights" with no significant change in slope, a fact of potential importance for stratospheric water vapor. A typical mixing ratio of the latter is 5 ppmv which corresponds, at 100 hPa altitude, to a volumetric extinction coefficient of about $5 \times 10^{-5}\mathrm{m}^{-1}$ assuming cloud particle diameters near 20–30 microns. This extinction level, indicated in Figure 1, lies on average at least one kilometer above $Z_{\mathrm{lid}}(1)$. This indicates that the cloud material within 1 km above $Z_{\mathrm{lid}}(1)$, hence up to 2–3 km above Z_{11}, must be at least partially tropospheric in origin and cannot be, for example, a pileus cloud formed from lower stratospheric air.

[10] The second interesting feature, indicated schematically in Figure 1 based on the results of *Heymsfield et al.* [1991] and *Sherwood et al.* [2004], is that the GOES radiometric cloud top Z_{11} colocated with the lidar retrievals lies at least 1 km below $Z_{\mathrm{lid}}(1)$. Those authors were unable to explain this discrepancy, but both studies noted that it was common to more than one infrared imager, so it is unlikely to be an instrument problem.

[11] Taken together, these facts indicate that true "cloud top" (defined in terms of visible opacity) must lie at least 1 km above (and stratospherically significant water vapor must typically be lofted to perhaps 2 km above) the cloud tops seen by GOES-8. Since these errors and/or processes are not well understood, we do not attempt to "correct" our height estimates, but instead beseech the reader to bear the problem in mind when interpreting our own (and others') thermal height estimates.

3. Computation of Thermal Cloud Heights

[12] To obtain reasonable statistics we must rely upon GOES-8 for cloud-top height information, subject to the caveats noted above. To obtain Z_{11}, the cloud "top" height according to passive radiances near 11 microns, we match brightness temperatures T_{11} obtained from GOES radiances to inferred temperature profiles (see below). The T_{11} were obtained from 4-km infrared (10.8 μm) observations every 15 min by the eighth Geostationary Operational Environmental Satellite (GOES-8). Calibration of the GOES-8 infrared radiances is maintained using onboard blackbodies. The GOES-8 data have also been compared with radiances from similar channels on two research satellites [*Minnis et al.*, 2002] and agree to within ±0.5 K over the full range of temperatures, on average. Cloud heights were determined by methods described by *Sherwood et al.* [2004], recounted below in sections 3.1 and 3.2.

[13] In this study we are interested in convective clouds, but make no effort to distinguish cloud types or to identify individual "clouds" or cloud systems. We simply count all pixels. We rely on the well-known relationship between cloud optical thickness and type [e.g., *Rossow and Schiffer*, 1991], with convective clouds having the highest water contents and opacities, and deep convective (typically Cb) clouds in particular accounting for the deepest optically thick clouds and lowest T_{11} values. Our height-determination procedure will automatically underestimate the heights of most nonconvective clouds due to their finite emissivities. This actually helps our analysis by reducing their contribution to the tail of the Z_{11}distribution, our primary focus. Further, any stratiform clouds opaque enough to register significantly in our results must be very fresh convective outflows and thus will occur at a height determined by that of the parent system. We will consider only pixel counts over large areas, described below, so that the aggregate height behavior in the data should well reflect that of the cumulus activity.

3.1. Regions and Satellite-Sounding Matching

[14] We computed Z_{11} statistics over three regions: the PEN or Florida peninsula region (roughly the mainland south of Tampa), the KW or Key West region (the Keys plus nearby ocean), and the FAGA or Florida-area Gulf/Atlantic Ocean region not included in KW. Each region is shown in Figure 2. A reference temperature profile was computed for each region and time as follows. For the KW region, the Key West sounding taken at the nearest available observing time was used; for the PEN region, the soundings from Miami, the Western Ground site, and Tampa at the nearest available observing time were averaged; and for the FAGA region, all four stations were averaged. The temperature profile for FAGA is therefore not expected to faithfully represent details of local atmospheric stability and CAPE. However, since the different stations reported very similar temperatures synoptically above the boundary layer, significant cloud height errors are unlikely from temperature variability and heights should be almost as good in FAGA as the other regions. We include the FAGA region mainly because of its larger size and better cloud statistics, and as a baseline against which to compare the other, smaller regions. The mean temperature soundings from the experiment are shown for KW and PEN in Figure 3.

[15] The sounding system in KW used the VIZ/Sippican B2 radiosonde with a carbon hygristor sensor, while the others used the Vaisala RS90. This may introduce a systematic difference in CAPE and LNB between the KW and

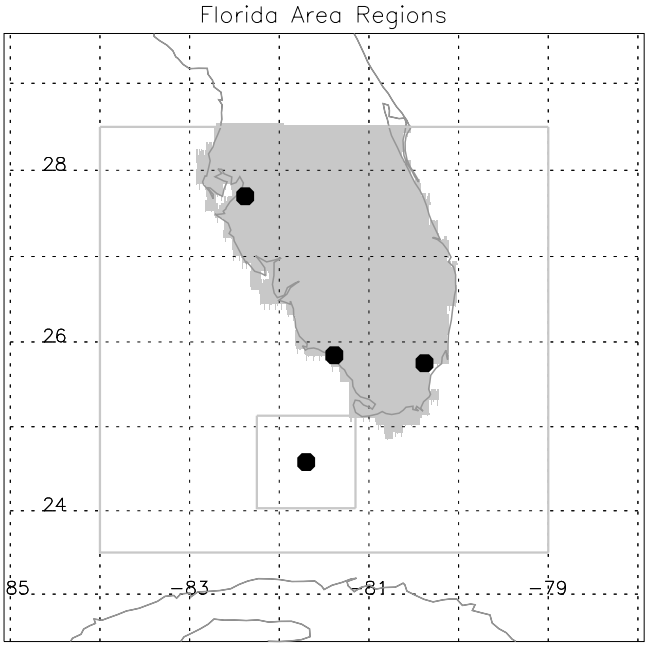

Figure 2. PEN region (shaded), KW region (square box), FAGA region (remainder of large box, excluding PEN and KW).

PEN regions, though it is unlikely to contribute significantly to differences in tropopause or cold point characteristics. This issue is revisited when discussing results.

[16] The "nearest available observing time" is taken to be the closest time of day at which there is at least one observation available from the station(s) in question. If no observations were available the entire day (which was the case for the first and last days of the month), then an average was taken of soundings within two days of the target time. Finally, for purposes of finding Z_{11} the temperature profiles were smoothed slightly in the vertical using a moving weighted window of width 15 hPa, to reduce features comparable to or smaller than a photon mean free path.

3.2. Cloud Temperature Assumption

[17] A height Z_{11} was computed for each GOES-8 pixel using the appropriate reference profile. Typically, one simply assigns the pressure and altitude where the profile matches the 11 micron brightness temperature T_{11} (the level nearest the surface is used if there is more than one match). This implies an assumption that the cloud temperature will be the same as that of a distant environment at the same altitude. While the interior of thermals tends to be several K warmer than the environment, this anomaly decreases toward cloud top where air is being mechanically lofted against potentially stable stratification, and (according to numerical simulations, not shown) becomes a cold anomaly. For overshooting convective clouds the cold anomaly becomes large, reaching as much as 20 K or more in extreme cases [e.g., *Adler and Mack*, 1986]. The lowest cloud-top temperature we observed (on 21 July) was 196 K, about 6 K below the cold point. Such cases demand an alternative $T(Z)$ relation for the cloud.

[18] Not knowing exactly how to do this, we tried three candidate procedures. The first, or "adiabatic-1" profile involved replacing temperatures above the WMO (lapse rate) tropopause with an adiabat intersecting the observed profile at the tropopause level. The "adiabatic-2" profile was identical except starting 40 hPa below the WMO tropopause, found to be a sufficient distance so that the lapse rate is fairly close to an adiabat and cloud buoyancies are more likely to be neutral. Finally we consider a "semi-adiabatic" profile which is just the average of the adiabatic-2 and environmental temperature profiles, representing the likely result of a cloud actively mixing with its environment. Depending on which profile is used, for example, our 21 July extreme GOES-8 cloud top is up to 8 K colder than the local (lower stratospheric) environmental temperature and occurs somewhere from 105–130 hPa. Though these differences serve as an uncertainty measure, they do not necessarily bracket all possibilities.

4. Observed Cloud Heights and Sounding Variations

[19] Cloud-top heights might be expected to reflect the ability of near-surface air parcels to ascend. Typically, a near-surface parcel in the summertime Florida environment can achieve positive buoyancy if lifted a small distance above its starting level; when the buoyancy returns to zero again, the parcel has ascended to its level of neutral buoyancy or LNB. On its way to this level, the potential energy available for conversion to kinetic energy is the CAPE. If all this energy remains in the parcel and is converted without loss back to potential energy again during an overshoot, then the parcel will reach its level of maximum overshoot (LMO), where it will come momentarily to rest before beginning its fall back toward the LNB. Since most updrafts have kinetic energy much less than CAPE, energy is evidently lost. This can occur due to exchange of moist

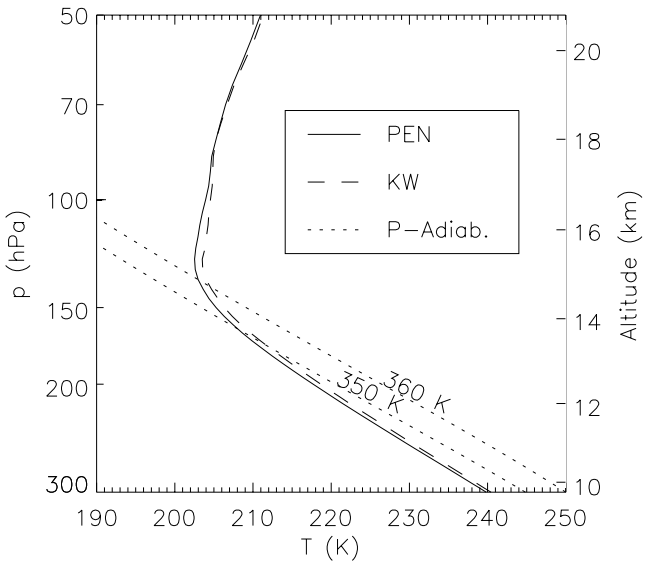

Figure 3. Mean temperature sounding for PEN and KW regions. Also shown are pseudoadiabatic profiles of a 350 and 360 K parcel. The intersections of these with the environmental profile is the LNB.

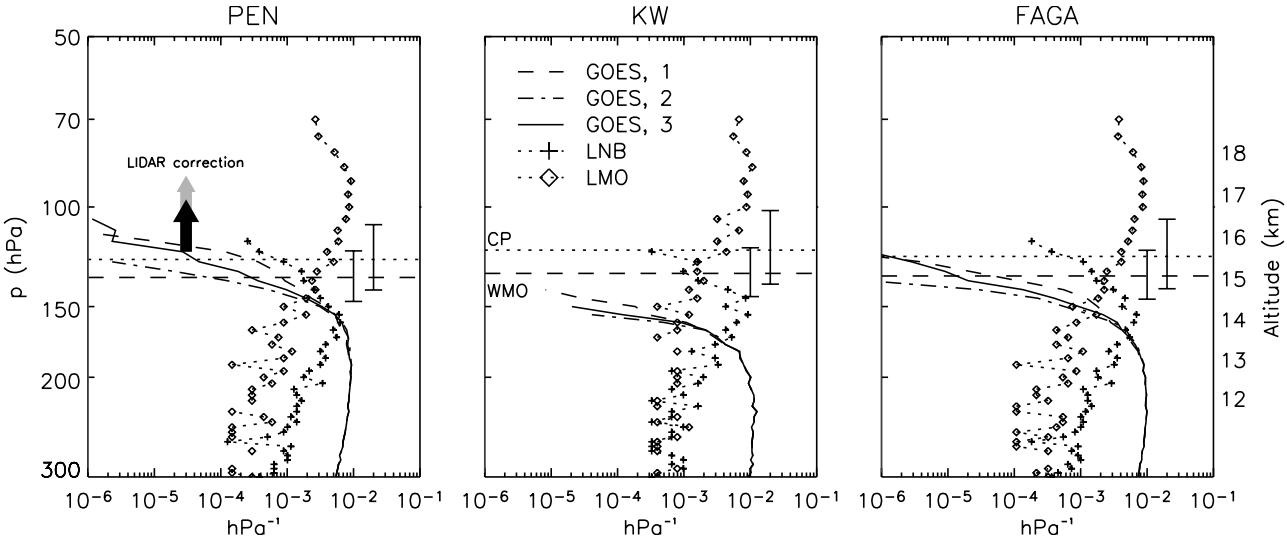

Figure 4. Height distribution of various parameters in the (left to right) PEN, KW, and FAGA regions. Solid lines show the density of p_{11}/Z_{11} observations from GOES using three different $T(Z)$ models: (1) tropopause adiabat (dashes), (2) tropopause +40hPa adiabat (dot-dash), and (3) semiadiabat (dot-dot-dash). Plus/diamond symbols show density (distribution) of pseudo-adiabatic LNB/LMO among parcels below 900 hPa. Mean location of WMO tropopause and cold point are shown by dashed and dotted lines, respectively, with standard deviations indicated by error bars. Thick dark arrow shows the additional altitude that must be added to Z_{11} to locate the visible cloud top in most cases; for the tallest clouds the discrepancy appears to increase to that shown by the gray arrow [*Sherwood et al.*, 2004].

enthalpy through mixing with the drier and/or cooler environment; mechanical transfer of momentum to the environment by mixing or drag; and/or lifting of precipitation against gravity. However, some parcels may occasionally avoid significant energy loss by unloading precipitation efficiently and/or remaining protected from mixing.

[20] Here, we will speak of the proportion of initial CAPE that the parcel successfully retains during this conversion process as the "efficiency," by analogy with the efficiency of thermodynamic engines. We have calculated LNB, LMO, and CAPE values assuming a pseudoadiabatic, irreversible and perfectly efficient ascent. We neglect latent heat of fusion to the ice phase. For CAPE purposes this has been shown to approximately compensate for the gravitational loading of condensate [*Williams and Renno*, 1993], which we also neglect, but our LNB altitudes would be somewhat higher if we took ice formation into account while allowing for the eventual unloading of all the condensate.

[21] We report the above quantities together with uncorrected cloud height variations observed by GOES. For the most part all will be reported as pressure (p_{11}) values, since the soundings measure pressure, but equivalent heights Z_{11} will be used interchangeably in the discussion (the $p(Z)$ relation varied little over the experiment). Readers should keep in mind that visible cloud-top heights are probably at least 1 km higher than Z_{11} (perhaps 2 km for the tallest examples), while significant amounts of condensed water may exist up to another kilometer above that. While a correction could have been incorporated into our plots by simply adding 1 km to each estimated height, we are loath to do this without understanding the error better. Future work with nonthermal height sensors will undoubtedly reveal more about the nature of these errors.

4.1. Height Distributions

[22] The distribution (histogram) of GOES p_{11} is shown in Figure 4 within each of the three regions. Also shown are vertical distributions of LNB and LMO, and the WMO tropopause and cold point mean locations, for each region. Comparison between the satellite and sounding distributions is necessarily crude, since our Z_{11} distribution is simply taken over all satellite pixels without worrying about the structure of the convective systems and variations of height within them. Similarly (and somewhat unconventionally), the LNB distribution is computed over all buoyant parcels between the surface and 900 hPa, at 20 hPa sampling resolution, without assuming a particular level of origin or performing vertical averaging. One can argue (neglecting cloud thickness variations for example) that both distributions are therefore weighted by the volume of buoyant air ingested into the cloud. This provides a basis for semiquantitative comparison.

[23] Clouds penetrated deepest over the peninsula (PEN). The histograms quickly begin falling off near 14 km (about 1 km below the WMO tropopause), but Z_{11} reached above the mean cold point height (15.4 km) in the most extreme cases. Different $T(Z)$ models lead to about a 1 km range in the extreme heights, causing the cold-point penetration frequency (based on Z_{11}) to range from about 0.01% to 1% of that at 14 km (which is not sensitive to the $T(Z)$ model). In view of the biases noted above, however, we presume that the fall off in visible cloud-top heights began

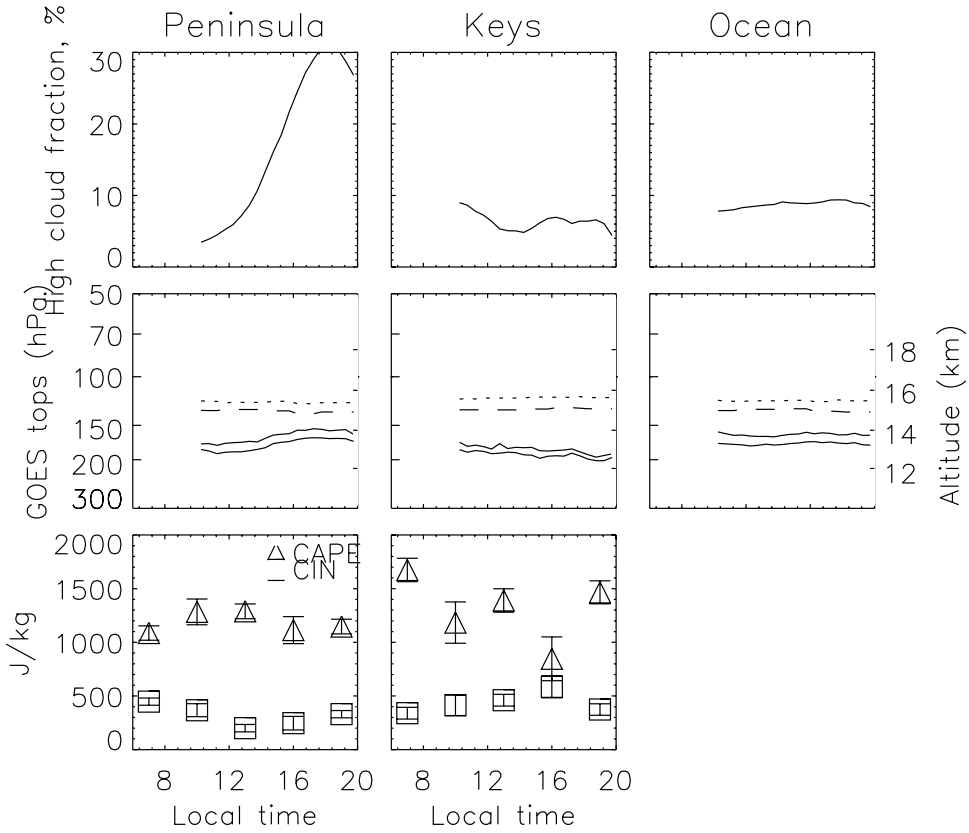

Figure 5. (top row) Fraction of GOES pixels within each region in which $T_{11} < 235$ K, versus local time of day. (middle row) The 5th (lower solid) and 0.20th (upper solid) percentile values of p_{11}/Z_{11} among those pixels below 235 K. Tropopause and cold point are indicated by dashed and dotted lines respectively. (bottom row) Variation of CAPE (triangles, left scale) and CIN (squares, left scale divided by ten) with standard errors. CIN values are truncated at 150 J/kg before averaging to improve the efficiency of the mean statistic (CAPE and CIN diurnal cycle not available for FAGA region). CAPE values are averages over all parcels having values greater than 100 J/kg.

right around the lapse-rate tropopause or cold point. This implies much more frequent cloud penetration of these levels than the values quoted above. Further, we may infer that stratospherically significant ice concentrations were occasionally inserted to heights up to 2 km above the cold point, or ~17 km. It is obviously difficult to be quantitative about cloud penetrations of the tropopause in the face of such large uncertainties in Z_{11} and its interpretation.

[24] The tails of the pseudoadiabatic LNB and Z_{11} distributions match fairly well in the PEN region, both tailing off near 160 hPa. Given the radiometric issues, this implies that the highest visible tops typically reached 1–2 km above the LNB. The LMO distribution peaked broadly near 100 hPa and reached as high as 19 km, greater than any observed height even taking biases into account, which probably indicates that no overshoots penetrated all the way to the theoretical LMO of a nonentraining parcel. However, given the apparent tendency of GOES to saturate toward the tallest clouds, it is hard to rule out very deep cloud penetrations with certainty.

[25] In the Key West (KW) region, the Z_{11} histogram resembles that over the peninsula except for a downward shift of about 1 km. Cloud-top frequencies begin falling off near 13 rather than 14 km, exhibiting a slightly more gradual or "rounded" fall off at first but achieving peak heights at least one kilometer lower than those over the peninsula. This difference persisted despite the fact that the average CAPE, LNB, and tropopause height were about the same. In fact, the tropopause and cold point were each slightly higher over KW. The reasons for the lesser cloud heights are not clear, but the difference is consistent with previous findings [*Jorgensen and Lemone*, 1989; *Lucas et al.*, 1994] that updraft speeds are greater in general for continental than for oceanic convection. It is particularly interesting that both regions possess histogram "bends," but at altitudes that do not seem simply related to the tropopause or LNB. It is possible that a modest CAPE difference between the regions could be masked by the sensor differences noted in section 3.1, but given the similar findings by earlier studies it is more likely that CAPE is indeed a poor predictor of geographical variations in cloud height.

[26] Cloud heights over the other nearby oceans (FAGA) were in between those of Key West and the peninsula. It is not clear why Key West cloud heights were depressed relative to other oceanic areas, though one likely possibility is that Key West is relatively close to the peninsula, whose stronger convection may inhibit that over nearby oceans.

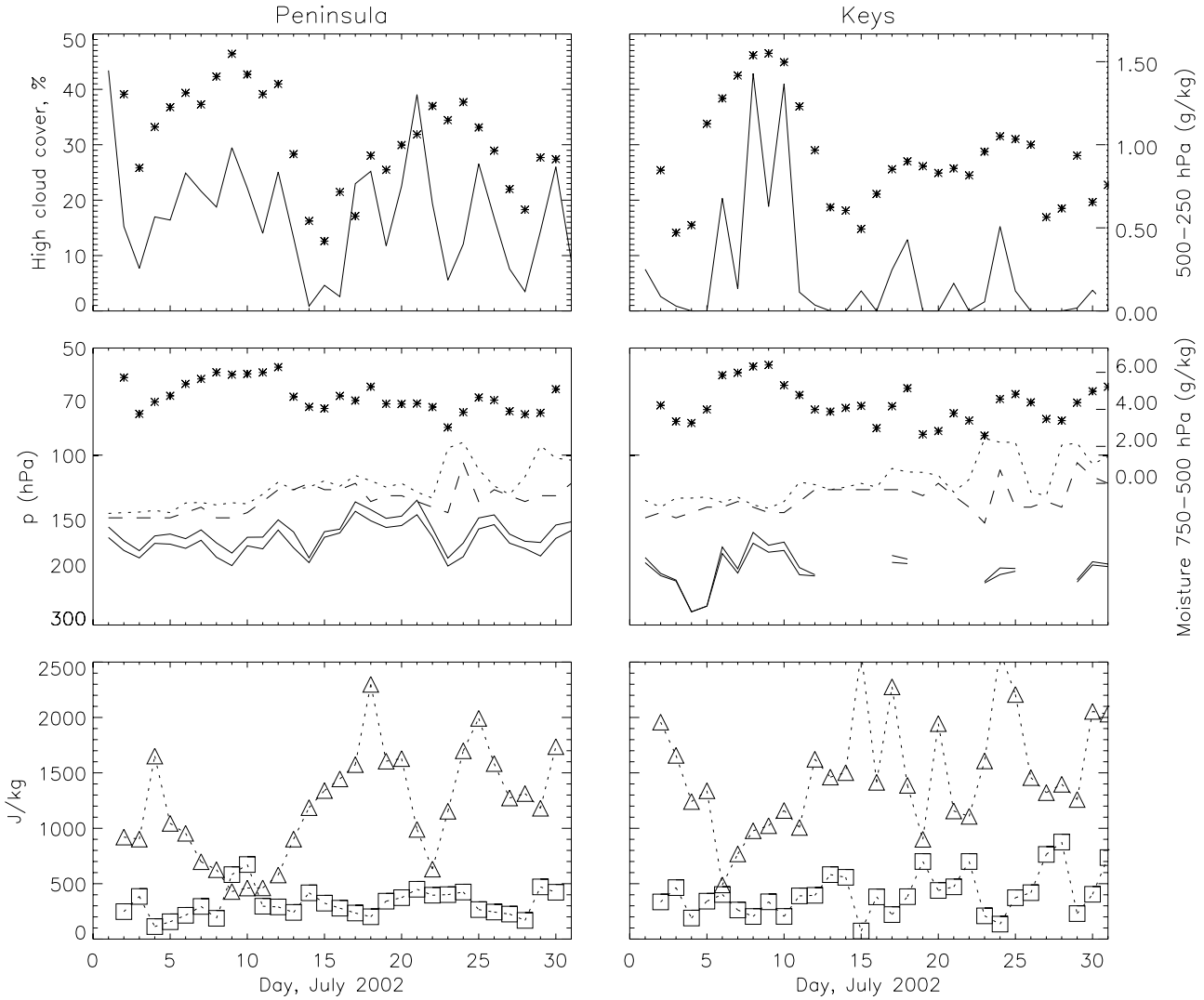

Figure 6. As in Figure 5 except abscissa is day of the month, and moisture variables have been added (scale at right) with asterisks: upper tropospheric moisture is added to the top row, middle tropospheric to the middle row. FAGA region not included owing to lack of sounding information.

Owing to the lack of sounding data over the oceans, it is not possible to assess differences in stability between these regions and Key West.

4.2. Diurnal Cycle

[27] Diurnal cycles of several quantities are shown for each region in Figure 5. The mean CAPE for a particular time of day is found by averaging over buoyant (CAPE >100 J/kg) parcels only. Results are similar, but with a lower mean, if all parcels are included. The diurnal variations of CAPE are small, with a slight peak in the late morning, while cloud height shows a strong afternoon peak over PEN. Thus the diurnal variation in cloud height over land is not explained at all by CAPE. The CAPE variations themselves are readily explained by solar heating and convective effects, with an afternoon dip accompanying the downward transport of cool air by convection.

[28] The true explanation of the diurnal cycle in convective coverage and penetration is well known to involve mesoscale dynamics. Morning sea-breeze fronts are created at the Florida coastlines, forming the locus for local-scale lifting and convection [*Estoque*, 1962; *Pielke*, 1974; *Burpee*, 1979; *Burpee and Lahiff*, 1984; *Shepherd et al.*, 2001; *Yuter and Houze*, 1995a]. The fronts typically propagate inward as density currents, depending on the synoptic wind situation, sometimes colliding in the early afternoon and producing even stronger convection. These mesoscale effects presumably also enhance cloud heights relative to the KW region. There are, however, several other factors that may contribute more generally to a broad and well-observed (but as yet not fully explained) difference between land and ocean convective intensity under similar CAPE situations [see *Lucas et al.*, 1994]. It is likely that modeling studies will be necessary to unravel the causes of this in general.

4.3. Day-to-Day Variations: LNB, LMO, and Moisture

[29] Parcel theory could still be successful in accounting for daily mean variations within a given region (Figure 6). Daily means of parcel properties are again calculated by

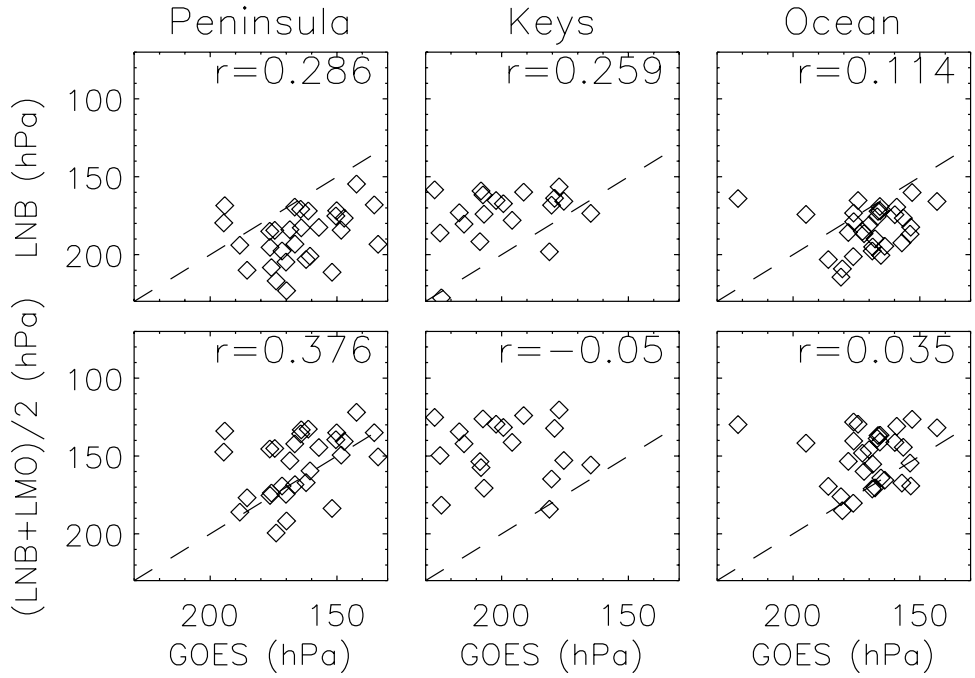

Figure 7. (top row) LNB and (bottom row) the average of LNB and LMO pressures versus 0.20th-percentile p_{11} from GOES, with each day represented by a symbol. Midtropospheric moisture is not accounted for. Dashed line shows equality, and r is the correlation coefficient including all points. LNB and LMO calculations for FAGA are based on coastal stations and are accurate only to the extent that variations in these quantities are of synoptic scale.

averaging over all buoyant, low-level parcels. In addition to quantities examined earlier, we now include mean water vapor mixing ratios in the lower (750–500 hPa) and upper (500–250 hPa) free troposphere. These mixing ratios include corrections for lag and bias errors [*Miloshevich et al.*, 2004].

[30] During the experiment, midtropospheric winds were generally light. A period of significantly disturbed weather occurred early in the month, during roughly 6–9 July over Key West and 8–12 July over the Peninsula. According to NCEP (National Centers for Environmental Prediction) reanalyses, not shown, this was associated with a moisture maximum originating over the Gulf of Mexico that slowly moved eastward, against the mean midtropospheric flow which was weak and easterly. This nearly stationary disturbance lingered in the region until abruptly propagating northeastward midmonth, after which midtropospheric moisture was generally lower. A second, shorter period of disturbed weather over the peninsula occurred just after this on 17–21 July, which included some of the highest CAPE values and deepest cloud tops and was coincident with particularly weak midtropospheric winds. This was followed by a relatively stable period, and a brief return of more active weather at the end of the experiment.

[31] The daily means show the expected correlations between high cloud cover, upper tropospheric water vapor, and midtropospheric water vapor, although each series shows some independence from the others. Greater amounts of high cloud cover (top row) also correlate with deeper cloud penetration (middle row), as one might expect if storm vigor were correlated with storm size or number. Finally, CAPE (bottom row) typically falls during maxima in high cloud cover, probably due to reduced solar heating and transport of cool air toward the surface, as has been reported elsewhere. These correlations are not sensitive to how the various variables are averaged or calculated.

[32] Most relevant to this study are those factors associated with convective penetration. CAPE appears to increase penetration somewhat as expected, though there are a number of counterexamples (4 July with high CAPE and modest Z_{11}, for example, or 14 July, where the reverse occurred). Interestingly, while CAPE appears to minimize a day too early to explain the low Z_{11} on 23 July, the 750–500 hPa moisture dips on just the same day as Z_{11}. Throughout the month, and in all regions, this moisture variable appears to track Z_{11} as well as, or better than, CAPE. While upper tropospheric moisture mirrors deep convective coverage (top row of the figure, and is for example high on 23 July), the 750–500 hPa moisture behaves differently and resembles cloud height more closely than cloud amount. This suggests that moisture variations are regulating cloud penetration in a way that is independent of variations in convective coverage or frequency.

[33] The connection between CAPE and cloud heights is investigated more carefully in Figure 7, which compares peak p_{11} against two indices based on parcel theory. The first index is the LNB pressure, while the second is the mean of the LMO and LNB. The second quantity was inspired by the more detailed convective model employed by *Sherwood and Dessler* [2001], in which overshooting convective air masses are created in the levels between the LNB and LMO by a mixing process with the environment: in such a process, changes in either the LMO or LNB should contribute to changes in peak cloud heights.

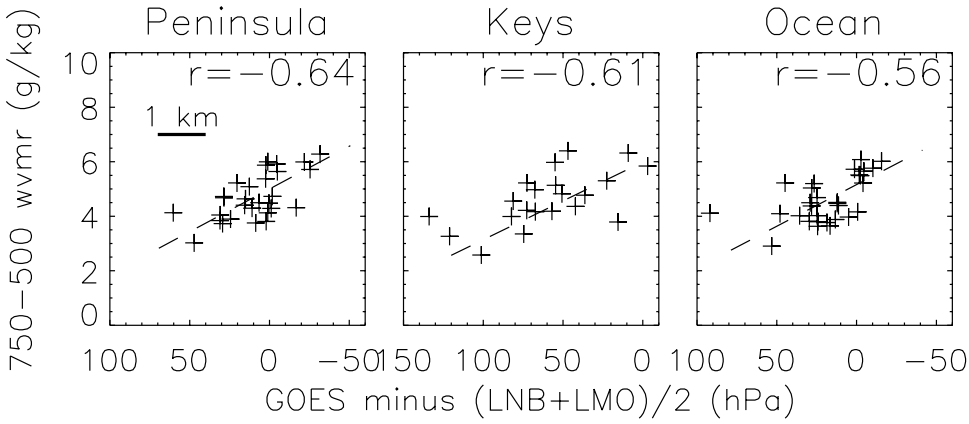

Figure 8. GOES p_{11} minus the mean of LNB and LMO pressures (x-axis), versus mean water vapor mixing ratio between 750–500 hPa (y-axis), for each region. Horizontal bar in left plot shows approximately 1 km of height difference, and the dashed line is drawn through the centroid of the points with a slope of 0.2 times the mean y axis value per kilometer. Note that FAGA moisture data are from coastal Florida and will be less representative than those for the other regions.

[34] The results confirm that the calculated LNB does (albeit loosely) track variations in observed cloud-top height, with about a one-to-one slope. The correspondence is best over PEN ($r = 0.29$). Interestingly, it is about as good over FAGA if a single outlier is excluded, even though the LNB is based on coastal data; this is probably due to horizontal coherence in the meteorology that causes CAPE variations. However, correspondence is poor over Key West and virtually disappears if a single outlier is discarded from that data set. This result makes sense if we accept the earlier explanation for why cloud tops were shallower over Key West (suppression from peninsular convection) since higher LNB's over Key West would correlate with higher ones over the peninsula and greater competition from convection there, potentially canceling out the local boost.

[35] If the LMO is included in predicting the cloud height, the mean value is estimated correctly over PEN and the correlation improves too (to $r = 0.38$). However, both the mean and correlation deteriorate over the oceanic regions. This is consistent with the apparently weaker convection over oceans, since significant convective overshooting is necessary before the theoretical LMO can have any impact.

[36] The relationship between midtropospheric moisture q_{mid} and observed cloud depth is explored in Figure 8, where the difference between the parcel theory result p_{mod} (the mean of LNB and LMO pressures) and observed p_{11} is plotted against q_{mid}. These correlations are highly significant everywhere ($r = -0.64$ for PEN, and almost as high for the oceanic regions, all significant at 95% confidence). Together, p_{mod} and q_{mid} explain about 30% of the day-to-day variance in p_{11} over the peninsula. By itself, q_{mid} explains 38% of the variance over Key West, but only 2% over PEN. Multiple regression of p_{11} onto both predictors over PEN yields partial correlations significant with p values of 0.92 for p_{mod} and 0.98 for q_{mid} respectively, providing fairly strong support for the idea that convective depth really is influenced independently by both factors. The unexplained residual time series completely decorrelates at a lag of two days (a fact employed in computing the above p values). This decorrelation lag is significantly shorter than those for the predictors themselves, suggesting that the remaining unexplained variability can practically be regarded as noise. This is encouraging for the prospect of predicting temporal, if not spatial, variability in convective depth using parcel theory including a moisture effect.

[37] The role of midlevel moisture in regulating convective outbreak, organization, and rainfall generation has been well documented in modeling and observational studies, in the Florida region and elsewhere [e.g., *Lin and Arakawa*, 1997; *Sherwood*, 1999; *Lucas et al.*, 2000; *Shepherd et al.*, 2001; *Tompkins*, 2001; *Grabowski*, 2003]. This role has typically been attributed to the entrainment of environmental air into the updraft, which reduces updraft buoyancy by an amount that depends on environmental relative humidity [e.g., *Malkus*, 1954; *Telford*, 1975; *Blyth*, 1993; *Barnes et al.*, 1996]. Our results add to the above by showing an apparent control of observed peak cloud-top heights by moisture above the boundary layer.

[38] The entrainment hypothesis can be quantitatively tested using parcel theory. The addition of 1 g/kg of moisture to a typical parcel of air adds about 3 K to its equivalent potential temperature, which for average conditions produces roughly a 20 hPa decrease in the pressure of the LNB. Of course, cloudy air must consist primarily of boundary-layer air mixed with only a fraction of environmental air, if it is to ascend through the whole troposphere; this implies that cloud LNB should change by significantly less than 20 hPa per g/kg increase in environmental moisture. However, in our data, 1 g/kg more environmental moisture is associated with about a 30 hPA lower cloud-top pressure relative to that predicted for a nonentraining parcel. The observed sensitivity exceeds that of even pure environmental air forced up to near-tropopause heights! We conclude that straightforward "parcel dilution" effects cannot be the whole story in explaining the impact of free-tropospheric moisture on cloud heights. The likely alternative is that dynamical feedbacks involving the reevaporation of lofted cloud and/or raindrops during the earlier stages of convective growth produce effects at later times that en-

hance the overall sensitivity. In particular, the entrainment rate experienced by the deepest drafts may end up larger when initial environments are drier. This would not be too surprising, given the impact of free-tropospheric moisture on convective organization in models [e.g., *Tompkins*, 2001]. The unfolding of this process from the congestus through the deep convective stage should be further investigated.

5. Conclusion

[39] We have examined histograms of convective cloud height near the tropopause, with the general goal of examining the tail of this distribution and assessing its sensitivity to environmental stability. All results must be viewed in light of the fact that "cloud top" is a fuzzy concept for deep convective clouds. Visible cloud tops based on direct lidar observations [*Heymsfield et al.*, 1991; *Sherwood et al.*, 2004] lie about one km higher than infrared ones (designated Z_{11}), perhaps up to 2 km higher for the tallest clouds. Further, cloud ice water concentrations typically remain "tropospheric" up to another kilometer above the visible top. All conclusions here are based on converting Z_{11} to putative visible tops by adding a constant offset of 1 km.

[40] Convective clouds penetrated about a kilometer deeper over the Florida peninsula than near Key West, with clouds elsewhere in the surrounding oceans falling in between. Peninsular clouds also exhibited a very strong diurnal cycle, as is well known. Neither the diurnal nor geographic variations in penetration seem to have anything to do with atmospheric CAPE, LNB, or tropopause properties, instead reflecting variations in the efficiency with which a parcel's CAPE is converted into its own kinetic energy (or, possibly, variations in the contributions of latent heat of fusion or energy spent lifting condensed mass). Previous studies have argued that land convection is stronger due to sea-breeze effects [e.g., *Burpee and Lahiff*, 1984], a deeper planetary boundary layer [*Jorgensen and Lemone*, 1989], aerosol influences on cloud microphysics [e.g., *Williams et al.*, 2002], and/or land surface elevation maxima [*Souza et al.*, 2000]. This question has not been fully resolved, though a consensus may be hoped for once regional numerical simulations incorporate sufficient microphysics, and become able to represent with sufficient fidelity the patterns to be explained.

[41] It is interesting that the histograms of cloud height in the different regions are so similarly shaped except for a 1-km offset between PEN and KW. For example, both show a quick bend toward lower frequencies above a particular altitude. One might expect the bend to be associated with increasing static stability near the tropopause, but this cannot be the case, as the bend altitude varied significantly with location, while the tropopause varied much less and in the opposite direction. Instead, the rough coincidence between the heights of steep lapse-rate change and convective tops is probably because of convective control of temperatures rather than stability-imposed convective "ceilings" [cf. *Sherwood et al.*, 2003; *Kuang and Bretherton*, 2004].

[42] The highest visible cloud tops over the peninsula were apparently located above the LNB by 1–2 km, and day-to-day fluctuations tracked those of both the LNB and LMO, although with considerable scatter. Much of the scatter was successfully explained by humidity variations just above the boundary layer (750–500 hPa). Under the null hypothesis of random cloud heights, there is only a 8% chance of obtaining the observed partial correlation with LNB/LMO over PEN (4% chance of also getting the physically expected sign), and a 1% chance of the same thing for midtropospheric moisture. Variations not explained by either predictor were consistent with random noise. This suggests that useful predictions of seasonal, interannual, and longer-term changes in cloud-top heights may be possible based on parcel theory. The evidence for this, however, is still not conclusive.

[43] The moisture impact is significant: we find that a 20% decrease in humidity above the boundary layer reduced peak cloud heights by about one kilometer, other things being equal. This happened over oceans too, where LNB variations are less relevant and LMO completely irrelevant. The magnitude of this impact is too large to result simply from the entrainment of drier air in an otherwise identical updraft, and must be due to feedback effects on the convective dynamics and/or entrainment rates. Future work should investigate carefully the evolution of environmental effects from the initial stages through to full-blown deep convection.

[44] An implication of this result is that relative humidities in the lower free troposphere can regulate the mean height of convective outflow, for a given atmospheric temperature structure and low-level moisture. This is important for upper tropospheric water vapor and its radiative feedback on climate change [e.g., *Hartmann and Larson*, 2002]. In particular, it is sometimes suggested that climate shifts could produce regions of enhanced subsidence and dryness, possibly altering the expected water vapor feedback on climate change. However, if this drying were to bring about a reduction in the intensity and height of convective outflow, as implied by the present work, this should reduce the drying impact of convection by redirecting outflows to warmer levels. Such a negative feedback would help to stabilize free-tropospheric relative humidity, but is obviously speculative at this point.

[45] All conclusions here rest upon the behavior of thermal cloud heights, which we are forced to assume are representative of the behavior of visible top heights despite the substantial (and, as yet, unexplained) bias between the two. Future studies may be able to improve on our results by making use of sufficient quantities of direct information on cloud height from stereoscopic or active sensors.

[46] **Acknowledgments.** We thank Heidi Zeleznik and Jung-Hyo Chae for help with data analysis, Larry Miloshevich for providing easy access to the raob data from CRYSTAL-FACE, and both reviewers for helpful comments. This work was supported by NASA EOS/IDS grant NAG-59632 and NSF grant ATM-0134893.

References

Adler, R. F., and R. A. Mack (1986), Thunderstorm cloud top dynamics as inferred from satellite observations and a cloud top parcel model, *J. Atmos. Sci.*, *43*, 1945–1960.

Adler, R. F., and A. J. Negri (1988), A satellite infrared technique to estimate tropical convective and stratiform rainfall, *J. Appl. Meteorol.*, *27*, 30–51.

Alcala, C. M., and A. E. Dessler (2002), Observations of deep convection in the tropics using the Tropical Rainfall Measuring Mission (TRMM) precipitation radar, *J. Geophys. Res.*, *107*(D24), 4792, doi:10.1029/2002JD002457.

Barnes, G. M., J. C. Fankhauser, and W. D. Browning (1996), Evolution of the vertical mass flux and diagnosed net lateral mixing in isolated convective clouds, *Mon. Weather Rev.*, *124*, 2764–2784.

Blyth, A. M. (1993), Entrainment in cumulus clouds, *J. Appl. Meteorol.*, *32*, 626–641.

Burpee, R. W. (1979), Peninsula-scale convergence in the south Florida sea breeze, *Mon. Weather Rev.*, *107*, 852–860.

Burpee, R. W., and L. N. Lahiff (1984), Area-average rainfall variations on sea-breeze days in south Florida, *Mon. Weather Rev.*, *112*, 520–534.

Chen, S. H., and W. Y. Sun (2002), A one-dimensional time dependent cloud model, *J. Meteorol. Soc. Jpn.*, *80*, 99–118.

Estoque, M. A. (1962), The sea breeze as a function of the prevailing synoptic situation, *J. Atmos. Sci.*, *19*, 244–250.

Ferrier, B. S., and R. A. Houze (1989), One-dimensional time-dependent modeling of GATE cumulonimbus convection, *J. Atmos. Sci.*, *46*, 330–352.

Fromm, M. D., and R. Servranckx (2003), Transport of forest fire smoke above the tropopause by supercell convection, *Geophys. Res. Lett.*, *30*(10), 1542, doi:10.1029/2002GL016820.

Gettelman, A., M. L. Salby, and F. Sassi (2002), Distribution and influence of convection in the tropical tropopause region, *J. Geophys. Res.*, *107*(D10), 4080, doi:10.1029/2001JD001048.

Grabowski, W. W. (2003), MJO-like coherent structures: Sensitivity simulations using the cloud-resolving convection parameterization (CRCP), *J. Atmos. Sci.*, *60*, 847–864.

Hartmann, D. L., and K. Larson (2002), An important constraint on tropical cloud-climate feedback, *Geophys. Res. Lett.*, *29*(20), 1951, doi:10.1029/2002GL015835.

Heymsfield, G. M., R. Fulton, and J. D. Spinhirne (1991), Aircraft overflight measurements of midwest severe storms—Implications on geosynchronous satellite interpretations, *Mon. Weather Rev.*, *119*, 436–456.

Jensen, M. P., and A. D. Del Genio (2003), Radiative and microphysical characteristics of deep convective systems in the tropical western pacific, *J. Appl. Meteorol.*, *42*, 1234–1254.

Jensen, E., D. Starr, and O. Toon (2004), Mission investigates tropical cirrus clouds, *Eos Trans. AGU*, *85*, 45–50.

Johnson, R. H., and D. C. Kriete (1982), Thermodynamic and circulation characteristics of winter monsoon tropical mesoscale convection, *Mon. Weather Rev.*, *110*, 1898–1911.

Jorgensen, D. P., and M. A. Lemone (1989), Vertical velocity characteristics of oceanic convection, *J. Atmos. Sci.*, *46*, 621–640.

Kuang, Z., and C. Bretherton (2004), Convective influence on the heat balance of the tropical tropopause layer: A cloud-resolving model study, *J. Atmos. Sci.*, in press.

Li, Y. (2003), Intensity of convective storms in Florida and their environmental properties, M.S. thesis, 128 pp., Univ. of Utah, Salt Lake City.

Lin, C. C., and A. Arakawa (1997), The macroscopic entrainment processes of simulated cumulus ensemble: 1. Entrainment sources, *J. Atmos. Sci.*, *54*, 1027–1043.

Lucas, C., E. J. Zipser, and M. A. Lemone (1994), Vertical velocity in oceanic convection off tropical Australia, *J. Atmos. Sci.*, *51*, 3183–3193.

Lucas, C., E. J. Zipser, and B. S. Ferrier (2000), Sensitivity of tropical West Pacific oceanic squall lines to tropospheric wind and moisture profiles, *J. Atmos. Sci.*, *57*, 2351–2373.

Malkus, J. S. (1954), Some results of a trade cumulus cloud investigation, *J. Meteorol.*, *11*, 220–237.

Miloshevich, L. M., A. Paukkunen, H. Voemel, and S. Oltmans (2004), Development and validation of a time-lag correction for Vaisala radiosonde humidity measurements, *J. Atmos. Oceanic Technol.*, in press.

Minnis, P., L. Nguyen, D. R. Doelling, D. F. Young, W. F. Miller, and D. P. Kratz (2002), Rapid calibration of operational and research meteorological satellite imagers, part II: Comparison of infrared channels, *J. Atmos. Oceanic Tech.*, *19*, 1250–1266.

Pielke, R. A. (1974), 3-dimensional numerical-model of sea breezes over south Florida, *Mon. Weather Rev.*, *102*, 115–139.

Rossow, W. B., and R. A. Schiffer (1991), ISCCP cloud data products, *Bull. Am. Meteorol. Soc.*, *72*, 2–20.

Shepherd, J. M., B. S. Ferrier, and P. S. Ray (2001), Rainfall morphology in Florida convergence zones: A numerical study, *Mon. Weather Rev.*, *129*, 177–197.

Sherwood, S. C. (1999), Convective precursors and predictability in the tropical western Pacific, *Mon. Weather Rev.*, *127*, 2977–2991.

Sherwood, S. C., and A. E. Dessler (2001), A model for transport across the tropical tropopause, *J. Atmos. Sci.*, *58*, 765–779.

Sherwood, S. C., T. Horinouchi, and H. A. Zeleznik (2003), Convective impact on temperatures observed near the tropical tropopause, *J. Atmos. Sci.*, *60*, 1847–1856.

Sherwood, S. C., J.-H. Chae, P. Minnis, and M. McGill (2004), Underestimation of deep convective cloud tops by thermal imagery, *Geophys. Res. Lett.*, *31*, L11102, doi:10.1029/2004GL019699.

Souza, E. P., N. O. Renno, and M. A. F. S. Dias (2000), Convective circulations induced by surface heterogeneities, *J. Atmos. Sci.*, *57*, 2915–2922.

Telford, J. W. (1975), Turbulence, entrainment and mixing in cloud dynamics, *Pure Appl. Geophys.*, *113*, 1067–1084.

Tompkins, A. M. (2001), Organization of tropical convection in low vertical wind shears: The role of water vapor, *J. Atmos. Sci.*, *58*, 529–545.

Williams, E., and N. Renno (1993), An analysis of the conditional instability of the tropical atmosphere, *Mon. Weather Rev.*, *121*, 21–36.

Williams, E., et al. (2002), Contrasting convective regimes over the Amazon: Implications for cloud electrification, *J. Geophys. Res.*, *107*(D20), 8082, doi:10.1029/2001JD000380.

Yuter, S. E., and R. A. Houze (1995a), Three-dimensional kinematic and microphysical evolution of Florida cumulonimbus, part I: Spatial-distribution of updrafts, downdrafts, and precipitation, *Mon. Weather Rev.*, *123*, 1921–1940.

Yuter, S. E., and R. A. Houze (1995b), Three-dimensional kinematic and microphysical evolution of Florida cumulonimbus, part II: Frequency distributions of vertical velocity, reflectivity, and differential reflectivity, *Mon. Weather Rev.*, *123*, 1941–1963.

Zipser, E. J., and K. R. Lutz (1994), The vertical profile of radar reflectivity of convective cells—A strong indicator of storm intensity and lightning probability?, *Mon. Weather Rev.*, *122*, 1751–1759.

M. McGill, NASA/Goddard Space Flight Center, Greenbelt, MD 20771, USA.

P. Minnis, NASA/Langley Research Center, Hampton, VA 23681, USA.

S. C. Sherwood, Department of Geology and Geophysics, Yale University, New Haven, CT 06520, USA. (ssherwood@alum.mit.edu)